Acta Oceanol. Sin., 2015, Vol. 34, No. 9, P. 71–77
DOI: 10.1007/s13131-015-0729-1
http://www.hyxb.org.cn
E-mail: hyxbe@263.net

The damping model for sea waves covered by oil films of a finite thickness

ZHANG Yanmin[1, 2], ZHANG Jie[1], WANG Yunhua[2]*, MENG Junmin[1], ZHANG Xi[1]

[1] The First Institute of Oceanography, State Oceanic Administration, Qingdao 266061, China

[2] College of Information Science and Engineering, Ocean University of China, Qingdao 266100, China

Received 18 August 2014; accepted 26 November 2014

Abstract

In combination with a wave action balance equation, a damping model for sea waves covered by oil films of a finite thickness is proposed. The damping model is not only related to the physical parameters of the oil film, but also related to environment parameters. Meanwhile, the parametric analyses have been also conducted to understand the sensitivity of the damping model to these parameters. And numerical simulations demonstrate that a kinematic viscosity, a surface/interfacial elasticity, a thickness, and a fractional filling factor cause more significant effects on a damping ratio than the other physical parameters of the oil film. From the simulation it is also found that the influences induced by a wind speed and a wind direction are also remarkable. On the other hand, for a thick emulsified oil film, the damping effect on the radar signal induced by the reduction of an effective dielectric constant should also be taken into account. The simulated results are compared with the damping ratio evaluated by the 15 ENVISAT ASAR images acquired during the Gulf of Mexico oil spill accident.

Key words: sea surface wave, oil film of finite thickness, damping ratio

Citation: Zhang Yanmin, Zhang Jie, Wang Yunhua, Meng Junmin, Zhang Xi. 2015. The damping model for sea waves covered by oil films of a finite thickness. Acta Oceanologica Sinica, 34(9): 71–77, doi: 10.1007/s13131-015-0729-1

1 Introduction

Oil pollution in the ocean environment is a matter of great concern because of the threats posed by such pollution to marine operations and wildlife. An effective surveillance of actively monitoring an oil film is necessary to avoid the oil pollution, more realistically, to keep it as small as possible. A remote sensing technology has been proved to be a powerful tool to detect and monitor oil spills films. In recent years, a microwave and optical systems have been utilized to detect oil films in the vast ocean. In particular, microwave synthetic aperture radar (SAR) has been shown to be very useful, because of the high spatial resolution and the insensitivity to cloud cover and daylight conditions. The oil films covering on the sea surface dampen the gravity-capillary waves, which are responsible for the reduction of the backscattered microwave signals, so the oil spills are observed as dark patches in the SAR images of the ocean surface(Migliaccio et al., 2005; Brekke and Solberg, 2005; Keramitsoglou et al., 2006; Liu et al., 2011; Minchew et al., 2012). The hydrodynamic theory of wave damping by the oil films of a negligible thickness (e.g., monomolecular films) has been established by Marangoni theory if very gentle wind regimes are in question (Hühnerfuss et al., 1983; Alpers and Hühnerfuss, 1989; Franceschetti et al., 2002; Pinel et al., 2008). The damping models proposed by Mallinger and Mickelson (1973) and Lombardini et al. (1989) and Wang et al. (1994) depend only on rheological parameters, such as the elasticity modulus and the characteristic frequency of the oil film. However, the presence of the oil film on the water surface reduces a friction wind velocity (Alpers and Hühnerfuss, 1989; Franceschetti et al., 2002; Gade et al., 1998; Kim et al., 2010). Therefore, the damping ratio is also closely related to the wind speed. To quantify the impact of the wind speed on the damping behavior, a physical damping model is proposed by means of the corresponding source functions in the wave action balance equation (Alpers and Hühnerfuss, 1989; Franceschetti et al., 2002; Gade et al., 1998; Kim et al., 2010). Using Marangoni theory and the wave action balance equation, the wave damping ratio by the monomolecular films can be reproduced. Here, it should be pointed out that a fractional filling factor, i.e., the ratio of the area covered by the film with respect to the total considered area, is also an import parameter need to be considered when calculating the damping ratio (Lombardini et al., 1989). In the general case, the thickness of a mineral oil spill is much larger than that of the monomolecular film, which results in different viscoelastic properties and, therefore, in different damping of the ocean surface waves. Thus, the reduction of the microwave backscatter from the sea surface covered with the oil film of the finite thickness is also of practical importance. However, the influence of the thickness of the oil film on the radar signal has not been widely investigated so far.

On the basis of the above analysis, the damping of the oil film would be related to several factors, such as the oil film thickness, the surface and interfacial tensions, the viscosity, the wind speed and the wind direction, the fractional filling factor, and so on. So, the exhaustive analysis about the wave damping ratio by the oil film is needed. Here, in combination with the wave action balance equation, a damping model for the sea waves covered by

Foundation item: The Young Scientists Fund of the National Natural Science Foundation of China under contract No. 41106153; China Postdoctoral Science Foundation Funded Project under contract No. 2012M521293.

*Corresponding author, E-mail: yunhuawang@ouc.edu.cn

the oil films of the finite thickness is proposed by utilizing the Jenkins and Jacobs (1997) wave viscous damping function (Jenkins and Jacobs, 1997). The parametric analyses of the damping model indicate that a kinematic viscosity, a surface/interfacial elasticity, the thickness, and the fractional filling factor cause significant effects on the damping ratio. On the other hand, the influences induced by the wind speed and the wind direction are also remarkable.

The remainder sections of the paper are organized as follows. In Section 2, the damping ratio of sea waves contaminated by the oil film of the finite thickness is proposed. And the parametric analyses are also performed to understand the sensitivity of the damping model to the parameters of the oil film and the environment. In Section 3, the results of our proposed damping model are compared with the measurement results by ENVISAT ASAR images. Finally, concluding remarks are provided in Section 4.

2 The damping model of sea surface waves

The radar signals from the sea surfaces covered by the oil spills of the negligible thickness (e.g., monomolecular films) have been widely studied (Alpers and Hühnerfuss, 1989; Mallinger and Mickelson, 1973; Lombardini et al., 1989; Wang et al., 1994; Pinel et al., 2008; Gade et al., 1998). Nevertheless, the thickness of the mineral oil spill is generally much larger than that of a monomolecular film, particularly, in the initial stages of an oil spill accident. Then, the radar signal reduction by the oil film of the finite thickness has practical significance, too. In a system which consists of a finite thickness film covering on a Newtonian fluid of the infinite depth, a damping ratio model for gravity-capillary waves is theoretically derived by Jenkins and Jacobs (1997) as follows:

$$y(k) = \frac{\mathrm{Re}(\delta)}{2\upsilon}, \tag{1}$$

with

$$\delta = \left\{ 2\upsilon + \frac{1}{2}\upsilon_{\mathrm{T}} + jT^{-1/2}[\gamma(1-\rho_+) - \gamma_-]D + \frac{1}{2\upsilon^{1/2} j^{1/2}}\rho + DT^{1/4}[\upsilon_{\mathrm{T}} + j\rho + DT^{1/2}(R^2-1)] \right\} \div (1 + \frac{1}{\upsilon^{1/2}T^{1/4}} j^{1/2}\upsilon_{\mathrm{T}} + \frac{1}{j^{1/2}\upsilon^{1/2}}\rho_+ DT^{1/4}), \tag{2}$$

$$\upsilon_{\mathrm{T}} = \frac{(\chi_+ + \chi_-)}{n} + \upsilon_{\mathrm{s}+} + \upsilon_{\mathrm{s}-} + 4\rho_+\upsilon_+ D + \frac{\upsilon_{\mathrm{E}+}\upsilon_{\mathrm{E}-}D}{\rho_+\upsilon_+}, \tag{3}$$

with

$$R = \frac{(\rho_+ + \gamma_+)}{\rho + T}, n = -j\sqrt{T}, T = 1 + \gamma, \gamma = \gamma_+ + \gamma_-,$$
$$\upsilon_{\mathrm{E}\pm} = \chi_\pm / n + \upsilon_{\mathrm{s}\pm},\ j = \sqrt{-1},$$

where k is the spatial wavenumber; τ is the tension of the sea water; υ is the kinematic viscosity of the sea water; ρ_+ is the density; γ_+ is the surface tension; γ_- is the interfacial tension; D is the thickness; υ_+ is the kinematic viscosity; χ_+ is the surface elasticity; χ_- is the interfacial elasticity; $\upsilon_{\mathrm{E}+}$ is the effective surface viscosity; $\upsilon_{\mathrm{E}-}$ is the effective interface viscosity; $\upsilon_{\mathrm{s}+}$ is the surface viscosity and $\upsilon_{\mathrm{s}-}$ is the interfacial viscosity. The values of the physical parameters for the oil film used in the numerical simulations are located in Table 1 (see Jenkins and Jacobs, 1997).

Table 1. Values of physical parameters of the oil film used in the present work

Water density/kg·m^{-3}	1 023
Oil density/kg·m^{-3}	900
Kinematic viscosity of water/m^2·s^{-1}	10^{-6}
Kinematic viscosity of oil/m^2·s^{-1}	10^{-4}
Surface tension/mN·m^{-1}	25
Interfacial tension/mN·m^{-1}	15
Surface elasticity/mN·m^{-1}	15
Interfacial elasticity/mN·m^{-1}	10
Surface viscosity/mN·m^{-1}	0
Interfacial viscosity/mN·m^{-1}	0

However, it should be pointed out that the damping ratio evaluated by Eq. (1) is only available for very gentle wind regimes because not only a viscous dissipation but also the wind speed, a nonlinear wave-wave interaction, and a wave breaking dissipation would induce significant influences on the damping behavior with the increase of the wind speed. In order to quantify these considerations, the evolution of a surface wave spectrum is described by an action balance equation (Alpers and Hühnerfuss, 1989; Franceschetti et al., 2002):

$$0 = \frac{\mathrm{d}N^i}{\mathrm{d}t} = S^i_{\mathrm{in}} + S^i_{\mathrm{nl}} - S^i_{\mathrm{vd}} - S^i_{\mathrm{br}}, \tag{4}$$

where $i \in \{\mathrm{o};\mathrm{w}\}$ and the superscripts (o) and (w) denote oil-covered and oil-free sea surface, respectively; and S^i_{in}, S^i_{nl}, S^i_{vd}, and S^i_{br} respectively represent source functions describing the wind input, nonlinear wave-wave interactions, viscous dissipation, and wave breaking dissipation. The spectral action density $N^i = (\omega/k)\,\psi^i$, ω is angle frequency and ψ^i indicates the surface roughness spectrum. For oil-free sea surface, ψ^{w} (Elfouhaily et al., 1997) can be written as

$$\psi^{\mathrm{w}}(k,\phi) = M(k)f(k,\phi), \tag{5}$$

where $M(k)$ is the isotropic part of the sea wave spectrum; and $f(k,\phi)$ denotes the angular function, in which ϕ is the angle between the wave spreading direction and the wind direction. Theoretical expressions for the source functions can be found in the literatures (Alpers and Hühnerfuss, 1989). In the present work, only the cases for low to medium wind speeds are in question, the impact of the wave breaking dissipation can be neglected. Here, the wind input term S^i_{in} (Alpers and Hühnerfuss, 1989) is expressed as

$$S^i_{\mathrm{in}} = \beta^i N^i, \tag{6}$$

where β^i is the wind wave growth rate and it can be described by

$$\beta^i = 0.04\cos\phi(\frac{u^i_*}{c_{\mathrm{p}}})^2\omega, \tag{7}$$

where c_{p} is the phase velocity of the considered wave; and ω denotes the angular frequency of the wave and can be defined by a dispersion relationship

$$\omega = \sqrt{gk + \frac{\tau k^3}{\rho_{\mathrm{w}}}}, \tag{8}$$

here g is the acceleration of the gravity; and τ and ρ_{w} denote the surface tension and the seawater density, respectively. The fric-

tional velocities u_*^i for oil-free and oil-covered areas are

$$u_*^{\mathrm{o}} = \xi\, u_*^{\mathrm{w}}, \tag{9}$$

$$u_*^{\mathrm{w}} = \sqrt{C_{10}} U_{10}, \tag{10}$$

where ξ is a coefficient due to the reduction of the friction velocity caused by the surface film, and Gade et al. (1998) suggested that an average ξ value equals 0.8. In the present work, we select the experimental expression proposed by Wu (1980) to evaluate the drag coefficient C_{10}, i.e.,

$$C_{10} = (0.8 + 0.06U_{10}) \times 10^{-3}, \tag{11}$$

where U_{10} is the wind speed at a height of 10 m.

The viscous dissipation term (Alpers and Hühnerfuss, 1989) in Eq. (4) is written as

$$S_{\mathrm{vd}}^i = 2c_{\mathrm{g}} \Delta^i N^i, \tag{12}$$

where c_{g} is the wave group velocity andnd the viscous damping coefficient Δ^i is written as (Alpers and Hühnerfuss, 1989)

$$\Delta^{\mathrm{w}} = \frac{4k^2\eta\omega}{\rho_{\mathrm{w}} g + 3\tau k^2}, \tag{13}$$

here η is the dynamic viscosity. Using Eqs (1) and (13), the viscous damping coefficient for an oil-covered sea surface can be written as $\Delta^{\mathrm{o}} = y(k)\Delta^{\mathrm{w}}$.

The nonlinear wave-wave interaction terms S_{nl}^i (Alpers and Hühnerfuss, 1989) can be written as

$$S_{\mathrm{nl}}^i = \alpha^i N^i, \tag{14}$$

with

$$\alpha^{\mathrm{w}} \approx -1.15\beta^{\mathrm{w}}, \tag{15}$$

$$\alpha^{\mathrm{o}} = \alpha^{\mathrm{w}} + \delta\alpha, \tag{16}$$

$$\delta\alpha = 2c_{\mathrm{g}}\Delta_{\max}^{\mathrm{o}} \left(\frac{k}{k_{\mathrm{M}}}\right)^{3/2} \left(\frac{u_*^{\mathrm{w}}}{u_{*,\mathrm{c}}}\right)^2, \tag{17}$$

and $\Delta_{\max}^{\mathrm{o}}$ denotes the maximal value of Δ^{o}; k_{M} is the Marangoni resonance wave number; $u_{*,\mathrm{c}}$ is the critical wind stress at which the nonlinear energy transfer has reached the level where it just balances the oil damping. And the critical wind stress is generally determined by an experiment (Alpers et al., 1989).

Substituting Eqs (6), (12) and (14) into Eq. (4), we can obtain that

$$\frac{\psi^{\mathrm{o}}(k,\phi)}{\psi^{\mathrm{w}}(k,\phi)} = \frac{\beta^{\mathrm{w}} - 2c_{\mathrm{g}}\Delta^{\mathrm{w}} + \alpha^{\mathrm{w}}}{\beta^{\mathrm{o}} - 2c_{\mathrm{g}}\Delta^{\mathrm{o}} + \alpha^{\mathrm{o}}}, \tag{18}$$

and the surface roughness spectrum for oil contaminated sea waves is

$$\psi^{\mathrm{o}}(k,\phi) = \psi^{\mathrm{w}}(k,\phi)/y\prime(k), \tag{19}$$

with

$$y\prime(k) = \frac{\beta^{\mathrm{o}} - 2c_{\mathrm{g}}\Delta^{\mathrm{o}} + \alpha^{\mathrm{o}}}{\beta^{\mathrm{w}} - 2c_{\mathrm{g}}\Delta^{\mathrm{w}} + \alpha^{\mathrm{w}}}. \tag{20}$$

Generally, the oil film may be partially dispersed by winds and waves, so a fractional filling factor, F (i.e., the ratio of the area covered by the film with respect to the total considered area) is introduced to modify the damping ratio. In this case, a modified damping ratio model $y\prime_{\mathrm{m}}(k)$ (Lombardini et al., 1989) can be written as

$$y\prime_{\mathrm{m}}(k) = \frac{1}{1 - F + F/y\prime(k)}. \tag{21}$$

Figure 1 gives the damping ratios for different physical parameters of the oil film, the film thickness D=0.1 mm in Figs 1a–e, and the other physical parameters of the oil film are given in Table 1. From Fig. 1, we can see that the damping ratio is insensitive to the oil density, the surface/interfacial tension and the surface/interfacial viscosity. However, the damping ratio would be obviously affected by the kinematic viscosity, the surface/interfacial elasticity and the thickness of the oil film. As shown in Fig. 1d, the damping ratio decreases with the increase of the kinematic viscosity, and the peaks of the damping ratio move to the lower spatial wavenumber. Figure 1e shows that the damping ratio increases with the increasing surface/interfacial elasticity, and the peaks of the damping ratio move to the lower spatial wavenumber, too. From Fig. 1f one can find that the damping ratio is insensitive to the thickness of the oil film when the thickness is less than approximately 0.01 mm. However, the effect of the film thickness becomes noticeable when it is increased to approximately 0.01 mm, and the damping ratio would increase on the whole with the increasing thickness.

From Fig. 2a, we can find that the damping ratio is very sensitive to the fractional filling factor. It is found that the damping ratio for the fractional filling factor being 1 is twice larger than the value of the damping ratio for the fractional filling factor being 0.9. The influences of the wind speed and the wind direction are illustrated in Figs 2b and c, respectively. We find that the damping ratio decreases with increasing wind speed, and increases with the wave spread azimuth angle. One reason for this phenomenon is that the higher the wind speed, the higher the wind input energy, hence, the weaker the Marangoni damping effect. The other reason is that the wave-wave interaction becomes stronger when the wave spread azimuth angle is small. And from Eqs (7), (14) and (18), it is easily concluded that the stronger the wave -wave interaction, the weaker the damping effect.

3 The evaluated damping ratio by SAR data

At moderate incidence angles, microwave scattering from the sea surface is mainly dominated by the contribution of Bragg scattering. And the first-order scattering coefficient from oil-free and oil-covered sea surfaces (Ulaby et al., 1982) can be written as

$$\sigma_{pp}^i = 16\pi k_{\mathrm{e}}^4 |g_{pp}|^2 \psi^i(k_{\mathrm{B}}, \phi_{\mathrm{B}}), \tag{22}$$

where σ_{pp}^i denotes the normalized radar cross-section (NRCS), $pp \in \{\mathrm{HH}, \mathrm{VV}\}, i \in \{\mathrm{o}; \mathrm{w}\}$, and the superscripts (o) and (w) denote oil-covered and oil-free sea surfaces, respectively; $k_{\mathrm{e}} = 2\pi/\lambda_{\mathrm{e}}$ is the wave number of the incidence microwave; k_{B} and ϕ_{B} represent the Bragg wavenumber and the azimuthal angle between the radar look-direction and the wind direction, and g_{pp}^i is a geometric factor,

$$g_{pp}^i = \begin{cases} \dfrac{\varepsilon_{\mathrm{r}} - 1}{\left(\cos\theta + \sqrt{\varepsilon_{\mathrm{r}} - \sin\theta}\right)^2} & \text{for HH} - \text{pol}, \\ \dfrac{(\varepsilon_{\mathrm{r}} - 1)[\varepsilon_{\mathrm{r}}(1 + \sin^2\theta) - \sin^2\theta]}{\left(\varepsilon_{\mathrm{r}}\cos\theta + \sqrt{\varepsilon_{\mathrm{r}} - \sin\theta}\right)^2} & \text{for VV} - \text{pol}, \end{cases} \tag{23}$$

where ε_{r} is the relative permittivity of sea surface. For dull (3–6 μm) and sheen oil films (0.3 to –0.6 μm), because the relative permittivity of oil is generally very small and the microwave could penetrate the oil film almost without absorbing and scattering, the echoes from the oil-covered sea surface are mainly contrib-

uted by the scattering fields from the underlying water waves. Thus, in Eq. (23), the relative permittivity for the dull and sheen oil-covered sea surface can be set $\varepsilon_r = \varepsilon_r^w$. For the thick emulsified oil, there is a mixture of oil with water in a relatively thick emulsified layer, the microwave could not penetrate the thick emulsified layer, then the relative permittivity in Eq. (23) should be set $\varepsilon_r = q\varepsilon_r^o + (1-q)\varepsilon_r^w$, where q is the oil-water volumetric weighting factor (Minchew, 2012). For the oil-free sea surface $\varepsilon_r = \varepsilon_r^w$. Here, ε_r^w and ε_r^o are the relative dielectric constants of sea water and crude oil, respectively. Using Eqs (18)–(22), the damping ratio of the NRCS between the oil-free and oil- covered sea surfaces are written as

$$\frac{\sigma_{pp}^w}{\sigma_{pp}^o} = \begin{cases} \dfrac{\psi^w(k_B,\phi_B)}{\psi^o(k_B,\phi_B)} = y_{rm}(k) & \text{for dull and sheen oil,} \\ \dfrac{|g_{pp}^w|^2\,\psi^w(k_B,\phi_B)}{|g_{pp}^o|^2\,\psi^o(k_B,\phi_B)} = y_{rm}(k)\dfrac{|g_{pp}^w|^2}{|g_{pp}^o|^2} & \text{for thick emulsified oil.} \end{cases} \tag{24}$$

For the case of the dull and sheen oil films contaminated water, the NRCS would be affected by the damping of the sea surface wave, and this effect has been discussed in Section 2; For the thick emulsified oil, besides the damping $y_{rm}(k)$ of the sea surface wave, the NRCS is also influenced by the reduction of the effective dielectric constant (Leifer et al., 2012). In Fig. 3, the damping of the NRCS caused by the reduction of the effective dielectric

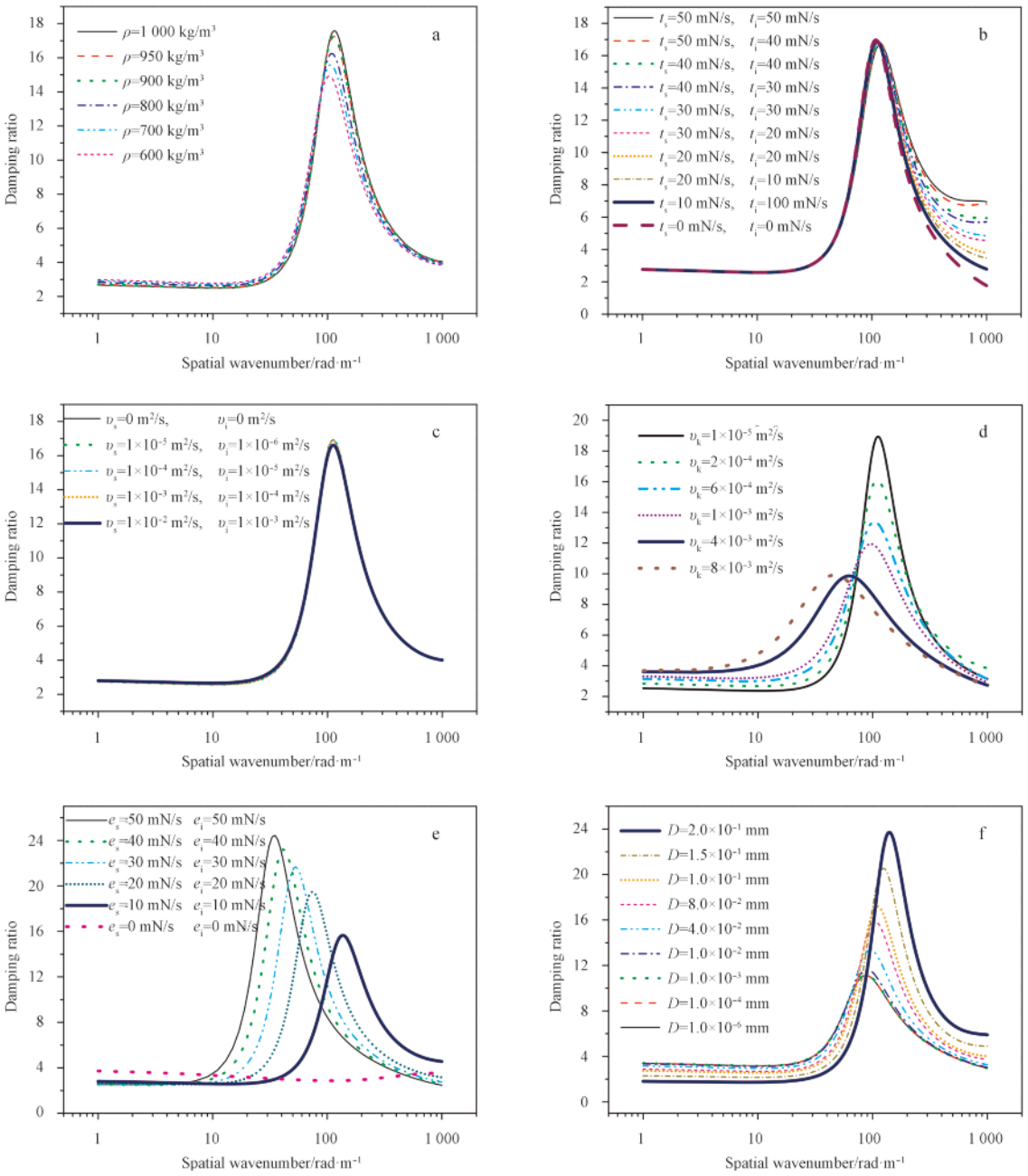

Fig. 1. Damping ratio of sea wave spectrum for different physical parameters of oil film with wind speed U_{10}=5 m/s, fractional filling factor F=1, and wave spread azimuth angle $\phi = 0^\circ$. a. For different oil densities ρ, b. for different surface tensions t_s and interfacial tensions t_i, c. for different surface viscosities υ_s and interfacial viscosities υ_i, d. for different kinematic viscosities υ_k, e. for different surface elasticities e_s and interfacial elasticities e_i and f. for different film thicknesses D of the oil film.

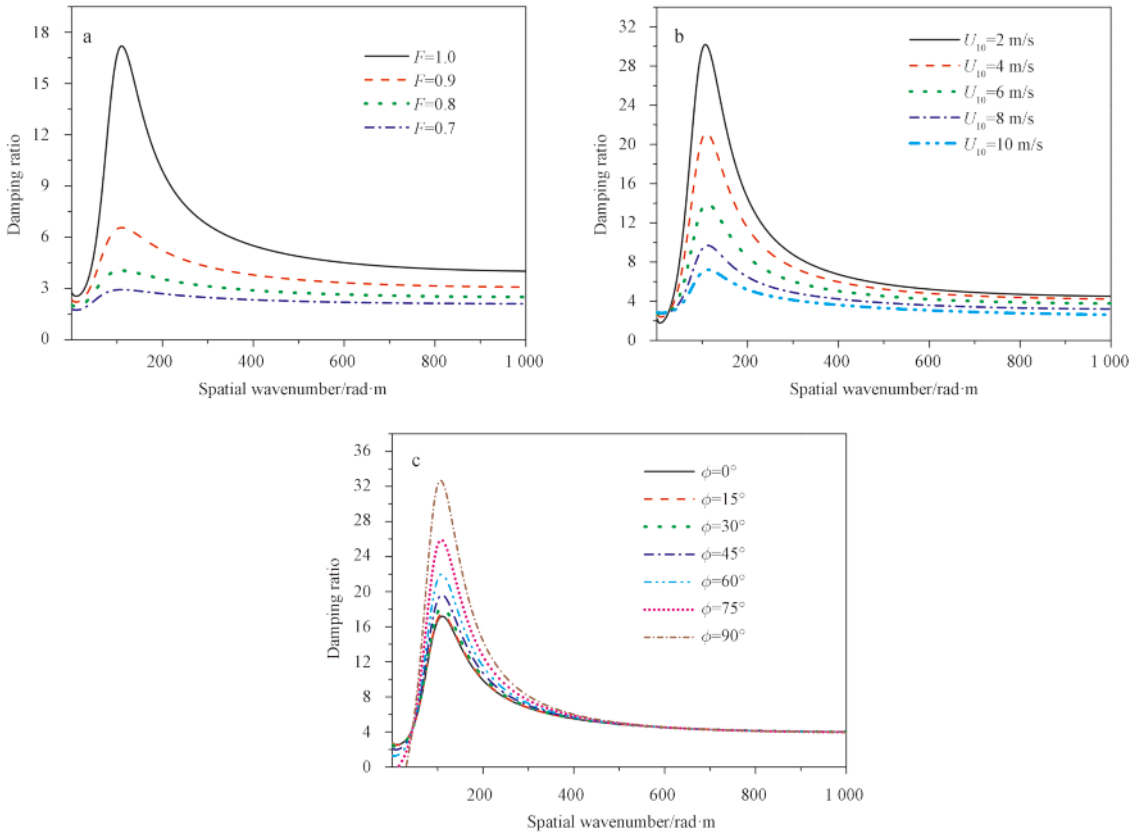

Fig. 2. Theoretical damping ratio evaluated by Eq. (21) for different environment parameters. a. For different fractional filling factors with wind speed being 5 m/s, film thickness being 0.1 mm and wave spread azimuth angle being 0°, b. for different wind speeds with film thickness being 0.1 mm, fractional filling factor being 1 and wave spread azimuth angle being 0°, and c. for different wave spread azimuth angles with wind speed being 5 m/s, film thickness being 0.1 mm and fractional filling factor being 1.

constant is shown for different polarizations. Here, the incidence angle θ=35°, the relative dielectric constants ε_r^w=65.67–i33.99 and ε_r^o=2.3–i0.02. From Fig. 3, we can see that $|g_{pp}^w|^2/|g_{pp}^o|^2$ increased with the factor q for VV and HH polarizations.

In the following, 15 ENVISAT ASAR wide swath mode images, which were acquired in the Gulf of Mexico during the 2010 BP oil spill accident, are used to evaluate the NRCS damping ratio. In Fig. 4, the SAR images have been labeled by the rectangle with borders, and the shadow region denotes the oil–spill-affected sea area. And the red star represents the location of NDBC Buoy 42040 at 29.212°N and 88.207°W which is the nearest buoys to the oil contaminated sea area. Here, the wind vectors acquired by Buoy 42040 are used in our simulations (the wind direction is coming from in degrees clockwise from true north).

As examples, three SAR images of the 15 ASAR images are shown in Figs 5a, c and e. And the corresponding NRCS along the red lines (azimuth direction) are shown in Figs 5b, d and f. From the figures, we can find that the NRCS has been distinctly decreased by the oil spill, and the evaluated damping ratios are different for these three SAR images. Further, we evaluated the damping ratio in the SAR images of Fig. 4, which are given in Table 2. The first column shows the acquisition time of the SAR image, the second column gives the wind vector measured by the buoy. And the third column is the average damping ratio evaluated by the SAR images.

Figure 6 shows the damping ratio versus the wind speed. The solid squares correspond to the damping ratios evaluated by the SAR images in Table 2, and the lines correspond to the theoretical damping ratios calculated by Eq. (20). The percentages of the total ocean surface oil coverage provided by NOAA and the USCG showed that the thick oil is 2%, dull oil film thickness (3 to 6 μm) is 10%, and sheen oil film thickness (0.3 to 0.6 μm) is 88% in the deepwater horizon oil spills accident (Labson et al., 2010). Moreover, in Fig. 6 the damping ratio evaluated by the SAR data is an average value. Then, in our simulations, the effect of the thick emulsified

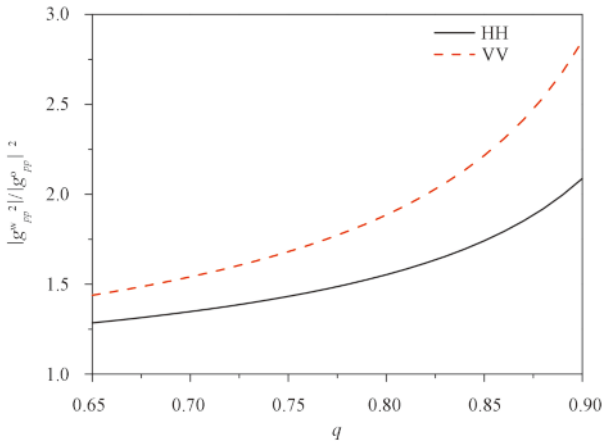

Fig. 3. $|g_{pp}^w|^2/|g_{pp}^o|^2$ versus oil-water volumetric weighting factor q.

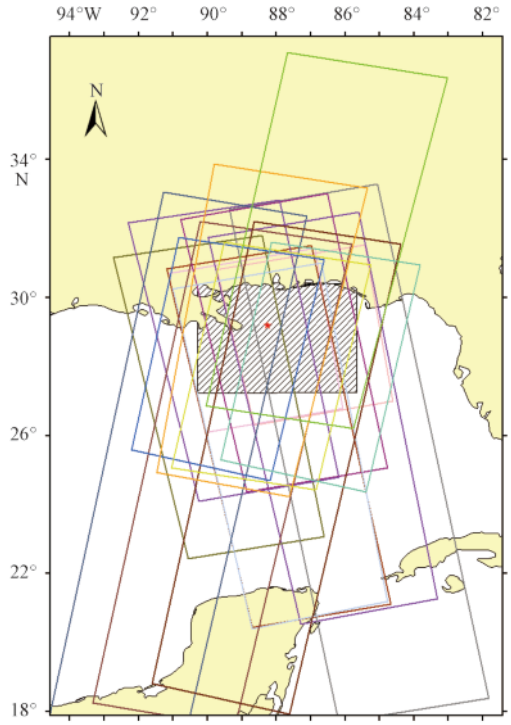

Fig. 4. ENVISAT ASAR images used to evaluate the damping ratio.

oil has been neglected. Considering the damping ratio is insensitive to the oil film thickness when the oil thickness is less 0.01 mm, we choose the oil thickness as 0.01 mm in the simulations.

From Fig. 6, we can see that the evaluated data with a lower wind speed agree the theoretical result with a higher oil fractional filling factors better, meanwhile the evaluated data with higher

Table 2. Damping ratios evaluated by SAR images

SAR images acquisition time (UTC)	Wind vector measured by buoy	Damping ratio
2010-04-29 03:45	3.2 m/s 187°	13.18
2010-05-02 03:51	9.7 m/s 153°	1.99
2010-05-02 03:51	9.7 m/s 153°	1.99
2010-05-09 15:48	8.7 m/s 57°	3.46
2010-05-12 15:55	7.1 m/s 115°	3.16
2010-05-25 15:47	4.9 m/s 118°	5.24
2010-05-28 15:52	2.8 m/s 314°	10.54
2010-06-03 03:56	4.9 m/s 147°	7.08
2010-06-06 03:49	4.3 m/s 194°	3.39
2010-06-09 03:56	5.5 m/s 132°	5.01
2010-06-22 03:48	4.7 m/s 143°	7.76
2010-06-25 03:53	3.9 m/s 113°	7.58
2010-07-11 03:49	6.4 m/s 210°	6.16
2010-07-18 15:49	5.0 m/s 163°	4.89
2010-07-21 15:55	7.3 m/s 93°	4.16
2010-07-24 16:01	4.5 m/s 61°	5.01

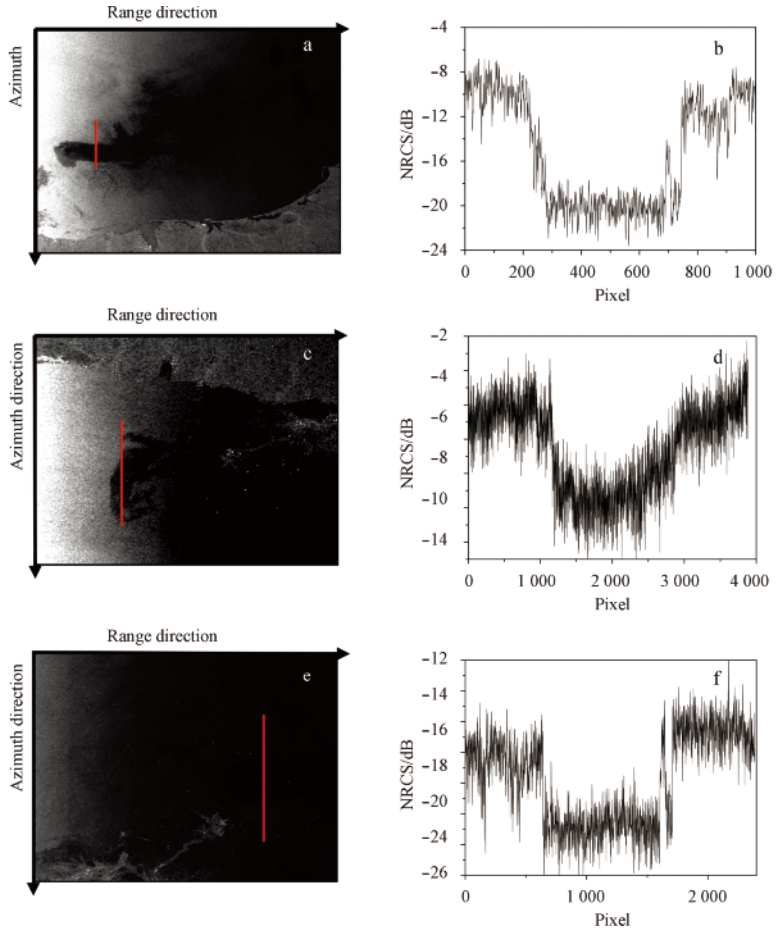

Fig. 5. Three SAR images acquired on 29 April 2010 at 12:55 UTC (a), 12 May 2010 at 15:55 UTC (c), 9 June 2010 at 03:56 UTC (e); and backscattered radar NRCS along the red scan line (azimuth direction) in a, c and e is given correspondingly in b, d and f.

wind speed agree the theoretical result with lower oil fractional filling factors better. And it seems reasonable that the fractional filling factor decreased with the increasing wind speed. The theoretical damping ratio can coincide with the evaluated data well when a suitable fractional filling factor is chosen for different wind speeds.

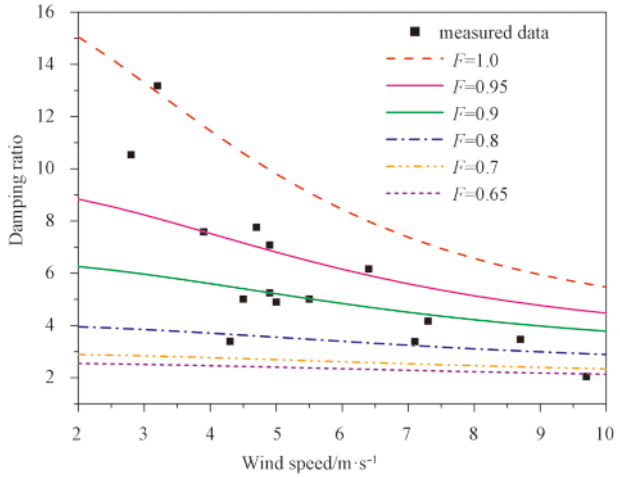

Fig. 6. The damping ratio versus wind speed.

4 Conclusions

In this paper, a damping model for sea waves covered by the oil films of finite thickness is proposed. The dependences of the damping ratio on the parameters of the oil film are discussed in detail. The numerical simulations show that the damping ratios are obviously influenced by the kinematic viscosity, surface/interfacial elasticity, thickness and fractional filling factor of the oil film. However, the damping ratios are almost insensitive to the oil density, the surface/interfacial tension and the surface/interfacial viscosity. In our simulations, the influences of the environment parameters, such as wind speed and wind direction, on the damping ratios are also discussed. It is found that the damping ratio decreases with the increasing wind speed, and increases with the wave spread azimuth angle. For the thick emulsified oil, the damping of NRCS by the reduction in the effective dielectric constant should also be considered. The damping model proposed in this manuscript is only a primarily theoretical work, and its validation should be verified in the future work.

Acknowledgements

The ENVISAT ASAR data were provided by the European Space Agency.

References

Alpers W, Hühnerfuss H. 1989. The damping of ocean waves by surface films: a new look at an old problem. J Geophys Res, 94(C5): 6251–6265

Brekke C, Solberg A H S. 2005. Oil spill detection by satellite remote sensing. Remote Sens Environ, 95(1): 1–13

Elfouhaily T, Chapron B, Katsaros K, et al. 1997. A unified directional spectrum for long and short wind-driven waves. J Geophys Res, 102(C7): 15781–15796

Franceschetti G, Iodice A, Daniele R, et al. 2002. SAR raw signal simulation of oil slicks in ocean environments. IEEE Transactions on Geoscience Remote Sensing, 40(9): 1935–1949

Gade M, Alpers W, Hühnerfuss H, et al. 1998. On the reduction of the radar backscatter by oceanic surface films: scatterometer measurements and their theoretical interpretation. Remote Sens Environ, 66(1): 52–70

Hühnerfuss H, Alpers W, Garrett W D, et al. 1983. Attenuation of capillary and gravity waves at sea by monomolecular organic surface films. J Geophys Res, 88(C14): 9809–9816

Jenkins A D, Jacobs S J. 1997. Wave damping by a thin layer of viscous fluid. Phys Fluids, 9(5): 1256–1264

Keramitsoglou I, Cartalis C, Kiranoudis C T. 2006. Automatic identification of oil spills on satellite images. Environmental Modelling & Software, 21(5): 640–652

Kim D J, Moon W M, Kim Y S. 2010. Application of TerraSAR-X data for emergent oil-spill monitoring. IEEE Trans Geosci Remote Sensing, 48(2): 852–863

Labson V F, Clark R N, Swayze G A, et al. 2010. Estimated minimum discharge rates of the Deepwater Horizon spill—interim report to the flow rate technical group from the Mass Balance Team. In: Salazar K, Mcnutt M M, eds. Science for a Changing World. Reston Virginia: US Geological Survey, 1–4

Leifer I, Lehr W J, Simecek-Beatty D, et al. 2012. State of the art satellite and airborne marine oil spill remote sensing: Application to the BP deepwater horizon oil spill. Remote Sensing of Environment, 124: 185–209

Liu Peng, Li Xiaofeng, Qu J J, et al. 2011. Oil spill detection with fully polarimetric UAVSAR data. Marine Pollution Bulletin, 62(12): 2611–2618

Lombardini P P, Fiscella B, Trivero P, et al. 1989. Modulation of the spectra of short gravity waves by sea surface films: slick detection and characterization with a microwave probe. J Atmos Ocean Technol, 6(6): 882–890

Mallinger W D, Mickelson T P. 1973. Experiments with monomolecular films on the surface of the open sea. J Phys Oceanogr, 3(3): 328–336

Migliaccio M, Tranfaglia M, Ermakov S A. 2005. A physical approach for the observation of oil spills in SAR images. IEEE J Ocea Eng, 30(3): 496–507

Minchew B. 2012. Determining the mixing of oil and sea water using polarimetric synthetic aperture radar. Geophys Res Lett, 39(16): L16607

Minchew B, Jones C E, Holt B. 2012. Polarimetric analysis of backscatter from the deepwater horizon oil spill using L-band synthetic aperture radar. IEEE Trans Geosci Remote Sensing, 50(10): 3812–3830

Pinel N, Déchamps N, Bourlier C. 2008. Modeling of the bistatic electromagnetic scattering from sea surfaces covered in oil for microwave applications. IEEE Trans Geosci Remote Sensing, 46(2): 385–392

Ulaby F T, Moore R K, Fung A K. 1982. Microwave Remote Sensing. Reading, MA, USA: Addision-Wesbey, 922–991

Wang Qingyu, Feder A, Mazur E. 1994. Capillary wave damping in heterogeneous monolayers. J Phys Chem, 98(48): 12720–12726

Wu Jin. 1980. Wind-stress coefficients over sea surface near neutral conditions—A revisit. J Phys Oceanogr, 10(5): 727–740